



A sustainable flow electrode capacitive deionization approach for efficient decontamination and uranium recovery from strongly acidic mining wastewater

Zhipeng Tang ^a, Yongmei Li ^{a,b,*} , Kaixuan Tan ^a, Chunguang Li ^{a,b}, Zhenzhong Liu ^{a,b}, Chong Zhang ^c, Haiwei Shi ^a, Le Ouyang ^a, Longcheng Liu ^{b,c,d}

^a School of Resource Environment and Safety Engineering, University of South China, Hengyang, 421001, China

^b R&D and Modelling Center for Treatment and Disposal of Radioactive Waste, University of South China, Hengyang, 421001, China

^c Beijing Research Institute of Chemical Engineering and Metallurgy, China National Nuclear Corporation, Beijing, 101149, China

^d Chemical Engineering, Royal Institute of Technology KTH, Stockholm, Sweden

HIGHLIGHTS

- FCDI was applied to treat strong acidic uranium mining wastewater.
- 95 % U removal efficiency and >80 % recovery rate were achieved under the optimal condition.
- U underwent electrochemical reduction, capacitive adsorption and complexation with AEM in FCDI.

ARTICLE INFO

Keywords:

In-situ leaching of uranium
Uranium-contaminated groundwater
Uranium recovery
Flow electrode capacitive deionization

ABSTRACT

The effective removal and recovery of uranium (U) from mining wastewater is of vital importance for environmental protection and the sustainable development of nuclear power industry. In this study, we applied flow electrode capacitive deionization (FCDI) to the treatment of uranium-contaminated groundwater generated after acid in-situ leaching (AISL). While FCDI has been previously explored for nutrient and heavy metal removal, as well as preliminary uranium extraction, this work uniquely demonstrates its effectiveness in strongly acidic, sulfate-rich mining wastewater, achieving >95 % uranium removal and >80 % recovery under optimal conditions. Theoretical calculations and experimental results reveal that U and coexisting ions in feedwater migrate rapidly to the cathode and anode during charging. UO_2^{2+} is electrochemically reduced to insoluble UO_2 on the carbon particles in the cathode, while $\text{UO}_2(\text{SO}_4)_2^{2-}$ is decomposed into $\text{UO}_2(\text{SO}_4)$ or UO_2^{2+} and SO_4^{2-} in the anode. After polarity reversal, the coexisting ions quickly transport into the spacer, while uranium is trapped in the cathode and anode, enabling selective uranium recovery. Long-term cycling tests using real mining wastewater confirms the FCDI system's high stability and material durability over 12 charging-discharging cycles. This study demonstrates FCDI as a promising technology for simultaneous uranium remediation and resource recovery from strongly acidic groundwater.

1. Introduction

Uranium, a natural occurring radioactive element, plays an important role in the nuclear fuel cycle. With the rapid development of nuclear energy, uranium mining has expanded rapidly in recent years. Notably, over 60 % of global uranium production is derived from sandstone-type uranium deposits through in-situ leaching (ISL) technology, as reported

by the International Atomic Energy Agency ([OECD-NEA & IAEA, 2020](#)).

In ISL mining, the leaching solution (usually sulfuric acid) is injected into the ore body through the injection well to dissolve the useful metals, and the uranium-containing solution is extracted through pumping wells to the surface for uranium recovery ([Bhargava et al., 2015; Zhou et al., 2020](#)). Despite its efficiency, acid in-situ leaching (AISL) inevitably leaves behind a large volume of strongly acidic, sulfate-rich

* Corresponding author. School of Resource Environment and Safety Engineering, University of South China, Hengyang, 421001, China.
E-mail address: lymusa8866@usc.edu.cn (Y. Li).

groundwater containing trace amounts of U(VI) (Maxim et al., 2016). For example, the groundwater at site post-AISL in Xinjiang, China, typically exhibits pH values below 2, sulfate concentrations of 5–10 g/L, and residual uranium concentration around 5 mg/L (He et al., 2021). This uranium-contaminated groundwater poses two critical challenges: (1) long-term environmental and radiological risks due to uranium mobility, and (2) the loss of valuable uranium resources in dilute aqueous forms. Consequently, there is a growing need for technologies capable of both remediating this wastewater and recovering uranium as a resource.

Several conventional approaches have been explored for uranium removal from contaminated water, including chemical precipitation, ion exchange, adsorption and membrane separation (e.g., reverse osmosis and electrodialysis) (Liao et al., 2004; Heshmati et al., 2015; Santos and Ladeira, 2011; Song et al., 2014). Chemical precipitation, ion exchange and adsorption are inefficient when treating contaminated groundwater with low uranium concentration, either due to high chemical demand or poor selectivity, as noted in previous study (Ke et al., 2023). Membrane separation methods such as reverse osmosis (RO) and electrodialysis often incur high energy consumption (Walha et al., 2007; Huang et al., 2022; Yang et al., 2025). For example, Lim et al. (2024) showed that the energy consumption of RO treating brackish water is about 0.8–2.7 kWh/m³ on a bench scale.

Capacitive deionization (CDI) has emerged as a promising technology for ion removal and resource recovery with the advantages of low energy consumption, chemical-free operation, and facile electrode regeneration (Jeon et al., 2013; Taulk et al., 2024a,b). However, traditional CDI systems using fixed electrodes are constrained by limited ion storage capacity and intermittent operation (Zhang et al., 2018). To address these problems, flow electrode capacitive deionization (FCDI) has been developed, wherein slurry-based flow electrodes enable continuous operation and near-infinite adsorption capacity (Ma et al., 2020; Zhang et al., 2020). Recent studies have demonstrated the applicability of FCDI for removing nutrients (e.g., N, P) (Xu et al., 2021; Chen et al., 2022) and heavy metals (Zhang et al., 2021; Zhong et al., 2024). Preliminary researches have suggested that uranyl (UO_2^{2+}), and uranyl complexes (e.g., $\text{UO}_2(\text{CO}_3)$, $\text{UO}_2(\text{SO}_4)$, $\text{UO}_2(\text{SO}_4)_2^{2-}$) can be effectively retained or transformed in FCDI systems (Ma et al., 2019; Zhou et al., 2022; Tang et al., 2025; Zhao et al., 2025).

Although FCDI has been investigated for removing various contaminants including nutrients, heavy metals, and uranium under simplified conditions, comprehensive studies on its performance in strongly acidic, sulfate-rich uranium mining wastewater remain scarce. In particular, the simultaneous evaluation of uranium removal, selective recovery, transformation mechanism, and long-term stability under such complex chemical environments has not been systematically reported. This study therefore focuses on addressing these gaps. First, the operational feasibility of FCDI under representative conditions of post-AISL groundwater was investigated. Then, the effects of key parameters (voltage, pH,

retention time, discharge time) on uranium removal and recovery performance under coexisting ions condition were explored. In addition, the migration and transformation mechanisms of uranium species within the FCDI device were analyzed. Finally, continuous cycling experiments on real post-AISL groundwater were conducted to assess stability, recovery efficiency, and material integrity. This work provides new insights into the electrochemical behavior of uranium under coexisting ions conditions and demonstrates the potential of FCDI as a sustainable solution for acidic uranium-contaminated groundwater remediation and resource recovery.

2. Materials and methods

2.1. Experimental setup

The configuration of the FCDI cell used in this study is depicted in Fig. 1. From the left to the right side, the acrylic end plate, graphite current collector, anion exchange membrane (AEM), silicone gasket inlaying with titanium mesh (0.5 mm thickness), cation exchange membrane (CEM), graphite current collector and acrylic end plate were placed in order and bolted together. The silicone gasket acted as the spacer or desalination chamber with the exchange membranes, enabling the flow of feedwater. Each graphite current collector was engraved with serpentine flow channel. The two ends of the flow channel (i.e., inlet and outlet holes) are connected to the pumping tube using a polyethylene connector. The parameters of each component of the FCDI device, including the size of the graphene current collector, the structure and size of the serpentine channel, and the technical specifications of the ion exchange membranes, were detailed in our previous work (Tang et al., 2025).

2.2. Experimental materials

Based on the physicochemical characteristics of mining wastewater in an uranium mine in Xinjiang, China, simulated acidic mining wastewater was synthesized using CaSO_4 , Na_2SO_4 , $\text{Fe}_2(\text{SO}_4)_3$, $\text{UO}_2(\text{NO}_3)_2 \cdot 6\text{H}_2\text{O}$, H_2SO_4 , and ultrapure water (18.2 MΩ·cm, Millipore). The ion concentration, conductivity and pH of simulated mining wastewater are shown in Table S1. The real mining wastewater sample was taken from an uranium mine in Xinjiang, the physicochemical parameters are shown in Table S2. The flow electrode consisted of 5 wt% activated carbon (AC) (YP-50, Kuraray, Japan), 1 wt% carbon black (CB) (ECP-Kochen Black-Japan) and ultrapure water (18.2 MΩ·cm, Millipore). To ensure that the carbon particles were fully wet, flow electrode was thoroughly stirred on a magnetic stirrer for 24 h before the experiment. All the chemical reagents used in this study were analytically pure unless otherwise stated.

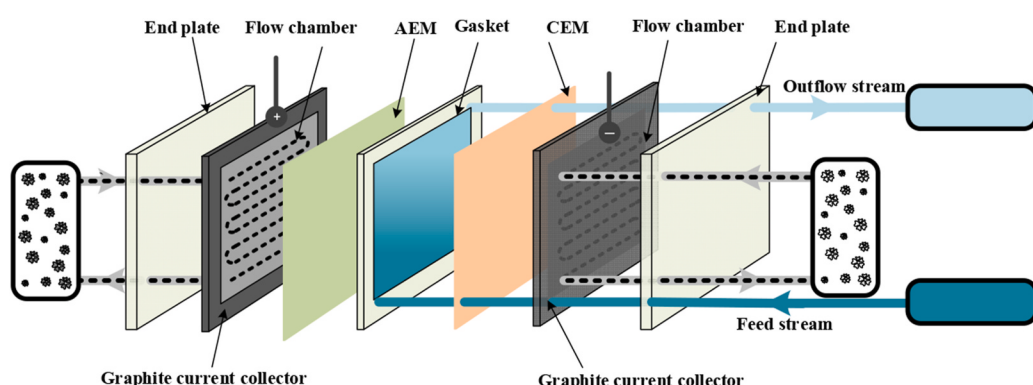


Fig. 1. Schematics of the FCDI system.

2.3. Experimental methods

In this study, we first assessed the feasibility of FCDI method to extract the uranium in acidic mining wastewater. The operational mode of isolated closed cycle (ICC)/single-pass was used, as displayed in Fig. 1. Electrode suspension of 50 mL on each side was recirculated between the flow electrode chamber and the stirred vessels at a flow rate of 40 mL/min. Synthetic mining wastewater as feedwater was pumped into the desalination chamber at a flow rate of 0.44 mL/min without circulation. A charging voltage of 3.6 V was applied to the two graphite collectors for 100 min to remove the contaminants from wastewater, afterwards, a reverse voltage of 0.2 V was applied to discharge for 30 min for U recovery. Three consecutive charging-discharging cycle tests were carried out by this means. Then, the effects of hydraulic retention time (1.26 min, 2.54 min, 5 min), charging voltage (1.2 V, 2.4 V, 3.6 V, 4.5 V), discharging voltage (0.2 V, 0.4 V, 0.6 V), discharge time (10 min, 20 min, 30 min), and synthetic mining wastewater pH (1.30, 1.65, 2.00) on the removal and recovery efficiency of uranium were investigated. During discharge, fresh synthetic mining wastewater was introduced into the spacer to simulate continuous operation. Under reverse polarization, most coexisting ions (Ca^{2+} , Fe^{3+} , Na^+ , etc.) were released from the flow electrodes into the spacer and mixed with the fresh feed, while uranium was selectively retained within the electrode chambers (as UO_2 deposited on cathodic carbon particles or U complexes desorbed into the anolyte). Thus, uranium recovery in this study refers to the selective enrichment of U in the electrode suspensions and membranes, rather than in the spacer effluent.

Electrochemical workstation was used as power, which can also record the current across the FCDI device in real time. The pH value of the anode and cathode electrode suspension was measured by pH meter, while the redox potential of the cathode electrode was continuously monitored by the ORP meter. The conductivity of water flowing out of the spacer was determined by Mettler multi-parameter instrument (S400-B). Ag/AgCl reference electrode (R0302, Shanghai Huayu) was inserted into the additional relay for in-situ measurement of the cathode electrode potential. The cathode potential in this study referred to the cathode electrode potential during charging, which is converted to anode during discharging, unless otherwise stated. A sample was collected from the effluent of the spacer at a fixed time (every 20 min during charging and every 10 min during discharging) for the determination of ion concentration.

The experiments in section 3.2.1 and 3.2.2 were performed for three times ($n = 3$), while other experiments, including several cycles, were performed as single operational replicates ($n = 1$) due to the complexity, especially the long term cycle experiment. However, the analytical measurements (ICP-OES, IC) were all performed in technical triplicate by the instrument. After each experiment, the ion exchange membranes were soaked with 2 % diluted nitric acid and sonicated for 20 min, and the flow channels of the graphite current collectors were flushed with 2 % HNO_3 followed by ultrapure water. This mild rinse was used solely to remove loosely bound electrolyte residues and prevent cross-contamination between cycles. The graphite current collectors were reused throughout all tests. No measurable mass loss of the collectors occurred after rinsing. The electrode suspension was filtrated by 0.22 μm filter (SCRC, China) to separate the carbon particles and electrolyte. The concentration of U(VI) and other ions in the electrolyte was determined. The carbon particles obtained were washed by ultrapure water and then dried under vacuum. The surface morphology and chemical composition of them were analyzed by scanning electron microscope combined with energy spectrometer (SEM + EDS), and the valence of uranium on carbon particles was determined by X-ray photoelectron spectroscopy (XPS). A Fourier infrared spectrometer was used to analyze the functional groups of carbon particles.

The concentration of U(VI) and other cations (Ca^{2+} , Fe^{3+} , Al^{3+} , Na^+) in water was determined by ICP-OES (Avio 220 Max, the detection limit for U is 15 $\mu\text{g/L}$), the Fe^{2+} concentration of water was measured by 1,

10-phenanthroline method (Xia et al., 2020), and the concentration of anion was determined by ion chromatography (IC 6100, RSD $\leq 1.0\%$ for SO_4^{2-}). In this study, Visual MINTEQ 4.1 software was used to analyze the species of U(VI) in water.

2.4. Calculations

Specific energy consumption (SEC, Kwh m^{-3}) can be calculated by the following equation (Xu et al., 2021),

$$\text{SEC} = \frac{\int_0^{t_c} I_c U_c dt + \int_0^{t_d} I_d U_d dt}{V_c + V_d} \quad (1)$$

where I_c and I_d are the current during charging and discharging process, respectively, (A); U_c and U_d are the cell voltages during charging and discharging process, respectively (V); V_c and V_d are the volume of feedwater during charging and discharging process, respectively (mL); t_c and t_d are the time of charging and discharging, respectively (min).

The removal efficiency of ion species i (R_i) during charging process was calculated by Eq. (2),

$$R_i = \frac{C_{0,i} - C_{c,i}}{C_{0,i}} \quad (2)$$

In this study, “recovery rate” (R_i^c) refers to the mass balance of ion species i between charging and discharging, as given by Eq. (3), which reflects the net mass of ions recovered during discharge.

$$R_i^c = \frac{m_c - m_d}{m_{total}} = \frac{(C_{0,i} - C_{c,i}) * V_c - (C_{d,i} - C_{0,i}) * V_d}{C_{0,i} * V_c} \quad (3)$$

where m_{total} is the mass of ion species i , m_c is the removed mass of ion species i during charge, m_d is the mass of ion species i transferred to spacer during discharge, $C_{0,i}$ is the initial concentration of ion i in mining wastewater, $C_{c,i}$ and $C_{d,i}$ are concentration of ion i in the effluent of spacer at the end of charging and discharging, respectively, (mg/L).

The average salt removal rate (ASRR_c , $\text{ug cm}^{-2} \text{min}^{-1}$) refers to the rate that ions migrate from the spacer to the flow electrode chamber during charging process. The average salt recovery rate (ASRR_d , $\text{ug cm}^{-2} \text{min}^{-1}$) represents the rate that ions migrate from the flow electrode chamber to the spacer during discharging process. ASRR_c and ASRR_d were obtained according to Eq. (4) and Eq. (5) (Chen et al., 2022),

$$\text{ASRR}_c = \frac{(C_{0,i} - C_{c,i}) \int_0^{t_c} f dt}{At_c} \quad (4)$$

$$\text{ASRR}_d = \frac{(C_{d,i} - C_{0,i}) \int_0^{t_d} f dt}{At_d} \quad (5)$$

where A is the effective contact area between flow electrode and ion exchange membrane, (cm^2), and f represents the flow rate of feed water, (mL/min).

3. Results and discussion

3.1. Feasibility analysis

Fig. S1 shows the conductivity of the effluent in three continuous charging-discharging cycle experiments. It is observed that the conductivity is rapidly reduced to less than 400 $\mu\text{S}/\text{cm}$ and remains stable within 100 min on condition of charging voltage of 3.6 V, but the conductivity rises quickly when a discharging voltage of 0.2 V was applied. This illustrates most of the ions are removed from the wastewater during charging process, and then migrate into the feedwater (fresh wastewater) during discharging process. **Fig. 2a** shows the removal and recovery efficiency of ions (U(VI), Ca^{2+} , Fe^{3+} , Na^+) versus charging/discharging time. It is clear that the removal efficiency of U(VI), Ca^{2+} , Fe^{3+} , Na^+ are very high ($\geq 97\%$). The recovery rate of Ca^{2+} , Fe^{3+} , Na^+

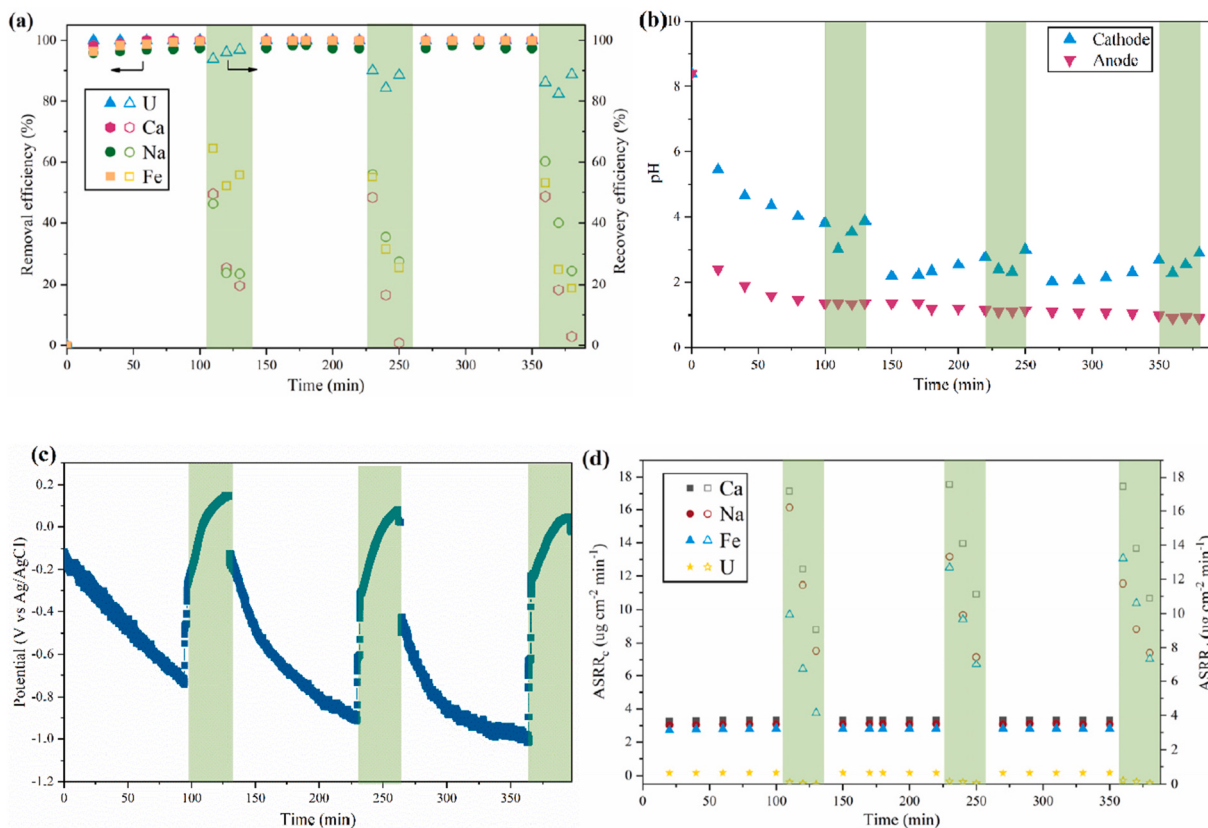


Fig. 2. (a) Removal efficiency and recovery rate of various ions (b) pH value (c) cathode electrode potential (d) average salt removal rate and average salt recovery rate. (Experimental conditions: $U_c = 3.6$ V; $t_c = 100$ min; $U_d = 0.2$ V; $t_d = 30$ min; HRT = 5 min) (The white part and light green part represents the charging and discharging process, respectively). (For interpretation of the references to colour in this figure legend, the reader is referred to the Web version of this article.)

decreases with discharging time, while the recovery rate of U(VI) remains relatively stable. In the second and third cycle tests, the recovery rate of U(VI) are 88.5 % and 88.7 %, respectively. By contrast, the recovery rate of both the total (Σ Fe) and Na^+ are around 25 %, and the recovery rate of Ca^{2+} is lower than 3 %. This implies uranium recovery is feasible by the FCDI installation.

Fig. 2b shows that the pH of anode flow electrode decreases with time in the first charging test, and then stays at about 1 in the latter cycles. It is interesting that the pH value of the cathode flow electrode reduces continuously during the first charging process, but it decreases first and then slightly increases in the second and third charging tests. In addition, it is seen from Fig. 2b that pH of the cathode flow electrode first decreases and then increases slightly during the discharging process. After three charging-discharging cycles, pH value of the cathode flow electrode remains at about 2~3.

The apparent inconsistency whereby the cathode pH decreases during the first charging test but increases in subsequent charging tests arises from dynamic changes in the local electrochemical environment rather than from experimental error. At the start of the first charge, rapid migration of H^+ from the strongly acidic spacer into the cathode lowers cathode pH (Fig. 2b). With continued operation, the cathode electrode potential relative to the silver chloride reference electrode becomes progressively more negative (Fig. 2c), and in later charging cycles it reaches values sufficient to electrochemically reduce H^+ to H_2 (visible gas evolution was observed in the experiment). This hydrogen evolution consumes protons and thereby raises the cathode pH in subsequent cycles. Concurrently, ionic accumulation and changes in the flow-electrode chemistry (e.g., increased electrolyte conductivity, and shifts in Fe redox state, see in Fig. S2b and Fig. S7) alter ohmic drops and overpotentials, allowing the cathode to attain more reducing potentials earlier in the charge stage during later cycles. Finally, conditioning of

carbon particle surfaces and the electric double layer after the first cycle modifies adsorption/buffering of H^+ , further changing the pH response. Together, these conditioning and electrochemical effects explain the observed transition from initial proton accumulation (first charge) to net proton consumption (later charges).

Generally, the anode electrode potential is high at charging stage, resulting in oxidation reaction, while the cathode electrode potential is low, then reduction reaction is prone to occur in cathode. It is observed from Fig. 2c that the cathode potential gradually becomes more negative with the increase of charging time in each test, indicating the enhanced reducing potential of the cathode. The cathode electrode potential decreases to -1.0 V (vs. Ag/AgCl) after the third charging test. Therefore, U (VI) is reduced to sparingly soluble $\text{UO}_2(\text{s})$ at cathode, while Fe^{3+} is reduced to soluble Fe^{2+} , and H^+ was reduced to H_2 , as shown in reaction (6)–(8) (Berenice et al., 2021; Wang et al., 2022; Ye et al., 2023; Guo et al., 2025). Though the cathode electrode potential increases gradually during discharging, it is still below $+0.2$ V after three charging-discharging cycles. Fig. S2b shows the fraction of Fe^{2+} that migrates from the cathode to the spacer at the end of discharging process. The portion of Fe^{2+} in the effluent after each discharging test was 60 %, 88 % and 87 %, respectively, suggesting that most of the Fe^{3+} migrating to the cathode chamber during charging process has been reduced to Fe^{2+} . Since the solubility constant K_{sp} of Fe^{2+} (4.87×10^{-17}) is much larger than that of Fe^{3+} (4.0×10^{-38}) (James, 2004), the reduction of Fe^{3+} in cathode is beneficial for the mitigation of membrane fouling. In addition, we found that many air bubbles are produced in the cathode, further demonstrating that H^+ is reduced to H_2 in the cathode.



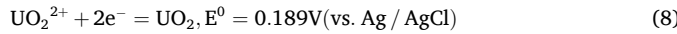
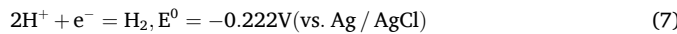


Fig. 2d shows the $ASRR_c$ and $ASRR_d$ of U (VI), Ca^{2+} , Fe^{3+} and Na^+ in the three charging-discharging tests. It's obvious that the $ASRR_c$ of each ion hardly changes with charging time in the three cycles, but $ASRR_c$ of Ca^{2+} , Fe^{3+} and Na^+ is several times larger than that of U. The reason is that the initial concentration of Ca^{2+} , Fe^{3+} and Na^+ is much higher than U concentration, while the final concentration of these ions are very low. It should be noted that $ASRR_d$ of Ca^{2+} , Fe^{3+} and Na^+ are much greater than $ASRR_c$ of these ions. In the third cycle, $ASRR_d$ of Ca^{2+} , Fe^{3+} and Na^+ is 17.46, 11.74, and $13.22 \mu\text{g}/(\text{cm}^2 \text{min})$, respectively, which are about 4~5 times as large as the $ASRR_c$ of these ions. This implies that Ca^{2+} , Fe^{3+} and Na^+ transport faster from the cathode chamber to the spacer at 0.2 V discharging voltage. This phenomenon is attributed to competition between ions. H^+ migrating to the cathode competes with Ca^{2+} , Fe^{3+} , and Na^+ during charging process, thus the migrate rate of Ca^{2+} , Fe^{3+} and Na^+ is slow though a charging voltage of 3.6 V was applied. However, a few H^+ entering the cathode is reduced to H_2 during charging process, that is, the H^+ content of the cathode flow electrode decreases, resulting in a weaker competition between H^+ and Ca^{2+} , $\text{Fe}^{3+}/\text{Fe}^{2+}$ as well as Na^+ during discharging process. Therefore, even a voltage of 0.2 V can promote the rapid migration of Ca^{2+} , Fe^{3+} and Na^+ from the cathode chamber to the spacer at discharging stage. Comparatively, the $ASRR_d$ of U is close to 0, indicating that U hardly returns to

the spacer during discharging. These results further suggest that uranium recovery is feasible using charging-discharging method.

3.2. Effects of the operational parameters on uranium removal and recovery

3.2.1. Hydraulic retention time and charging voltage

The conductivity of effluent can be effectively regulated by voltage and hydraulic retention time (HRT) (Luo et al., 2020). **Fig. 3a** shows that the conductivity of the effluent at steady-state decreases with the charging voltage at a given HRT. Under condition of a fixed charging voltage, the number of ions migrating to anode and cathode increases, but the ion replenishment of the spacer decreases with increasing HRT, resulting in a significant decrease in the conductivity of effluent and an increase in the internal resistance of the spacer. Therefore, for a specific charging voltage, the longer the HRT, the smaller the current across the FCDI device, as shown in **Fig. 3b**. As the charging voltage increases, the current across the FCDI device increases (**Fig. 3b**). It is observed from **Fig. 3c** that SEC increases with charging voltage at a given HRT. Furthermore, the prolongation of HRT slightly increases SEC. However, **Fig. 3d** shows that U(VI) concentration of the effluent decreases with the increase of HRT. The U(VI) concentration of effluent is lower than $300 \mu\text{g/L}$ (the emission limit in China) on condition of $HTR = 5 \text{ min}$ and $U_c = 3.6 \text{ V}$ or 4.5 V . To further determine the optimal charging voltage, the influence of charging voltages on the conductivity of effluent and the removal efficiency of ions were investigated at $HTR = 5 \text{ min}$ and $t_d = 30$

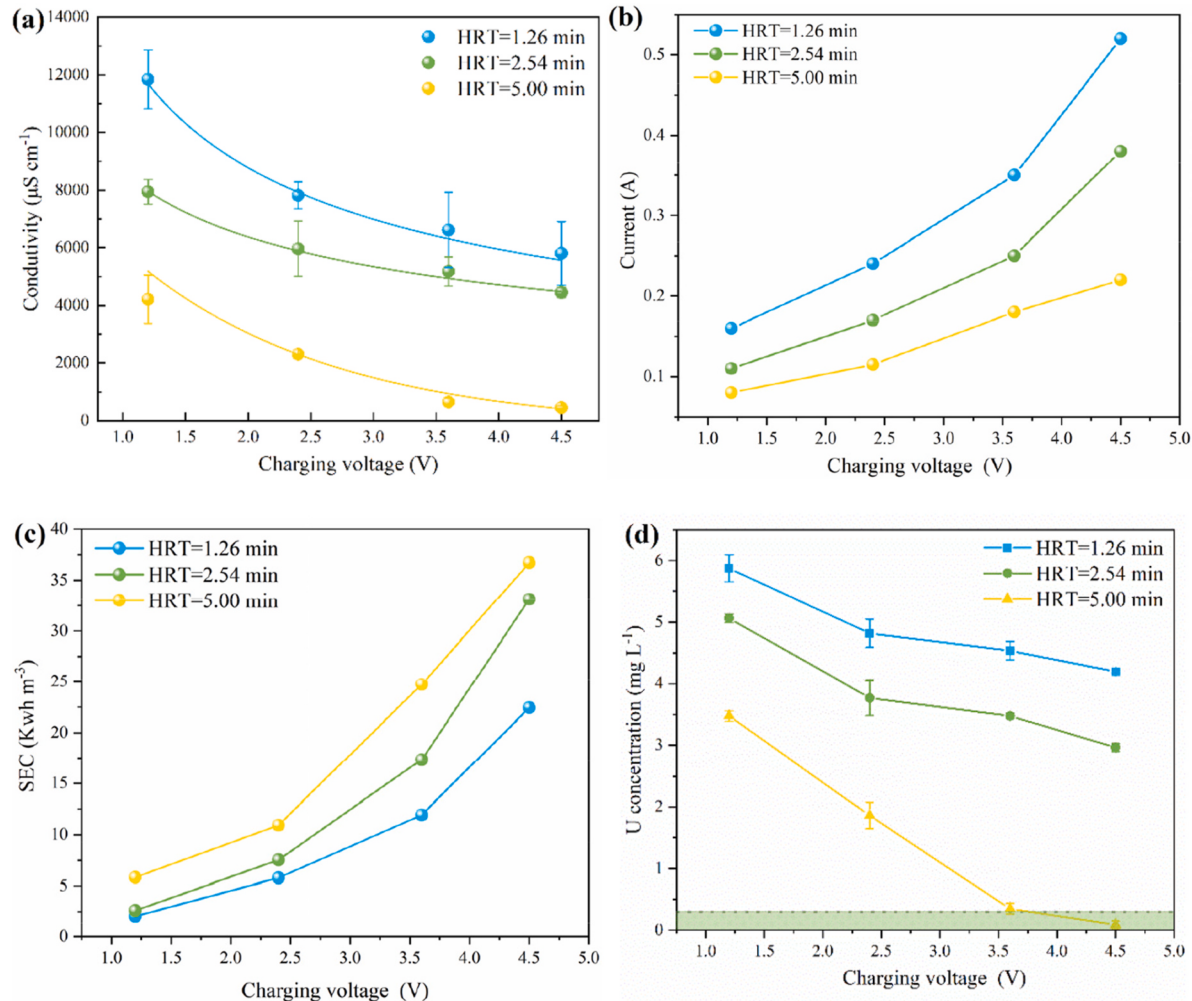


Fig. 3. (a) Conductivity of the effluent; (b) current across the FCDI unit; (c) specific energy consumption (SEC); (d) uranium concentration of the effluent at different charging voltages and HRT. (Experimental conditions: $t_c = 100\text{min}$; $U_d = 0.2\text{V}$; $t_d = 30\text{min}$).

min. The results are shown in Fig. S3. It's clear that the current across FCDI device, conductivity of effluent and the removal efficiency of ions hardly change with time during charging process ($t_c = 100$ min) when the charging voltage is 3.6 V or 4.5 V. The removal efficiency of all ions is above 90 % at charging voltage of 3.6 V or 4.5 V. Considering the removal efficiency (especially U (VI)) and the energy consumption of FCDI system, the charging voltage is better selected to be 3.6 V.

In CDI/FCDI, cell voltages above ~ 1.2 V are commonly associated with the onset of water electrolysis. In this study, the feedwater was both strongly acidic ($\text{pH} < 2$) and sulfate-rich, yielding high ionic strength and low spacer resistance. Under these conditions, the total cell voltage distributes across the two ion-exchange membranes, i.e., the spacer, and the two flowing slurries, then, substantial ohmic overpotentials are required to drive selective migration and transformation of U-species and decontamination of co-ions at practical residence time. As a result, operation at 3.6 V was necessary to achieve high removal efficiency of U and co-ions.

Side reactions were indeed observed, as discussed in section 3.1. During charging, the cathode potential became progressively more negative (to about -1.0 V vs Ag/AgCl, Fig. 2c), and visible gas formation was noted in the cathode chamber, indicating hydrogen evolution. This parasitic reaction, while incurring an energy penalty, consumed protons and thereby moderated cathode acidification over cycles and promoted the reduction of Fe^{3+} to Fe^{2+} , which helped limit membrane fouling caused by hydrolysis of multivalent cations.

3.2.2. Discharging voltage and time

Discharging voltage affects not only the migration rate of ions from the electrode chamber to the spacer, but also the electrode potential (Yin et al., 2023; Zhang et al., 2019), thus the influence of discharging voltage was investigated. Fig. 4a illustrates the conductivity of feedwater versus time during discharging process. At a specific discharging voltage, the conductivity of effluent increases rapidly over discharging time and then tends to be stable. Steady-state conductivity increases with increasing discharging voltage. The reason is that electrostatic repulsion between the carbon particles and ions is stronger at higher voltages, then, more ions would migrate from the cathode chamber to the spacer. It's observed from Fig. 4b that the recovery rate of uranium is the largest at $U_d = 0.2$ V. This is reasonable because higher discharging voltage like 0.4 V or 0.6 V might lead to enhanced oxidizability of the cathode, which would result in re-oxidation of some reduced UO_2 in the cathode, then, it would transport into the spacer due to acceleration of discharging voltage. As a consequence, uranium recovery rate is reduced.

Fig. 4c shows the redox potential of the cathode flow electrode (relative to the standard silver chloride electrode) as a function of discharging time. It is obvious that the redox potential of cathode flow electrode increases with discharging voltage and time. At the discharging voltage of 0.2 V, 0.4 V and 0.6 V, the redox potential increased to 70.5, 211 and 317 mV after 30 min of discharge, respectively. To interpret the speciation distribution of U at different redox potential and pH, the Eh-pH phase diagram of U in solution was obtained using HSC 9 software on condition of 25 °C, 1 bar total atmospheric pressure, and

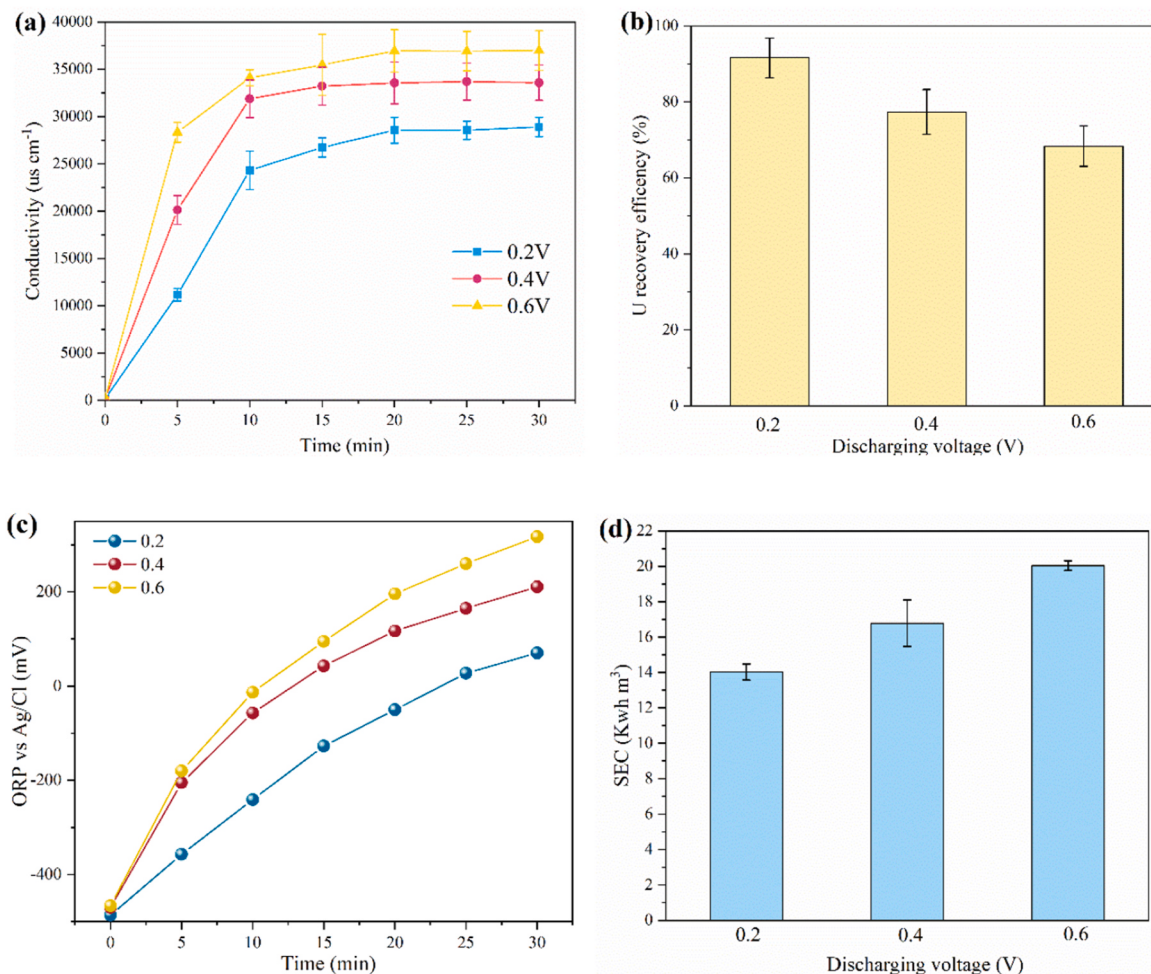


Fig. 4. (a) Effluent conductivity; (b) recovery rate; (c) redox potential; (d) volumetric energy consumption SEC at different discharging voltage. ($U_c = 3.6$ V, $t_c = 100$ min, $t_d = 30$ min, HRT = 5 min).

uranium concentration of 10 mg/L, which is close to the uranium concentration of the feedwater. The Eh-pH phase diagram of U is shown in Fig. 5. It is observed that the dominant speciation of U is slightly soluble UO_2 at potential below 150 mV, but UO_2^{2+} at potential above 150 mV, when pH of the cathode flow electrode is in the range of 2~3 (consistent with the pH of the cathode flow electrode at section 3.1). As can be seen from Fig. 4c, the redox potential of cathode flow electrode is always lower than 150 mV at discharging voltage of 0.2 V, thus, the dominant speciation of U is uncharged UO_2 under this condition, suggesting that discharge voltage of 0.2 V will not cause the UO_2 reduced during charging process to be oxidized again. This indicates that discharging voltage of 0.2 V is conducive to uranium recovery. In addition, the energy consumption of FCDI device is the lowest at discharging voltage of 0.2 V, being about $14.03 \pm 0.45 \text{ kWh/m}^3$ (Fig. 4d). Considering the recovery rate of uranium and the energy consumption of the FCDI unit, the optimal discharging voltage was 0.2 V, and the optimal discharging time was 30 min.

The SEC of FCDI in this study is higher than that of OR ($\sim 7 \text{ kWh/m}^3$) for brackish water with mineralization $>10 \text{ g/L}$ (Nassrullah et al., 2020). Based on the SEC at $U_d = 0.2 \text{ V}$, the electricity cost of FCDI is $\sim 1.4 \text{ USD m}^{-3}$ (assuming 0.1 USD kWh^{-1}). As we know, the energy consumption depends on feed salinity and recovery rate. Generally, the higher the salinity, the larger the energy consumption. Though cost of FCDI in this study is higher than those of RO ($\sim 0.7 \text{ USD m}^{-3}$) and ion exchange ($0.3\text{--}0.6 \text{ USD m}^{-3}$) for brackish water desalination, FCDI achieves simultaneously decontamination and U recovery for mining wastewater without chemical addition, moreover, it can recover $>95 \%$ of water, much higher than RO (Ma et al., 2023).

3.2.3. Initial pH of mining wastewater

It's well known that pH plays a critical role in uranium speciation, ion migration behavior, and redox reactions. The pH of groundwater in mining areas after acid in-situ leaching (AISL) is typically below 2 (He et al., 2021). To assess the influence of pH under realistic conditions, the initial pH of synthetic acidic mining wastewater (original pH = 1.30) was adjusted to 1.65 and 2.00 using dilute sulfuric acid. The FCDI system was then operated under the optimal conditions for five consecutive charging-discharging cycles to evaluate the initial pH of mining wastewater on uranium and coexisting ions behavior.

The removal efficiency of major ions at the end of the fifth cycle are shown in Fig. 6a. It is observed that the removal efficiency of U(VI) and coexisting ions remains above 95 % across all pH levels, confirming the robustness of FCDI system for contaminants removal in strongly acidic

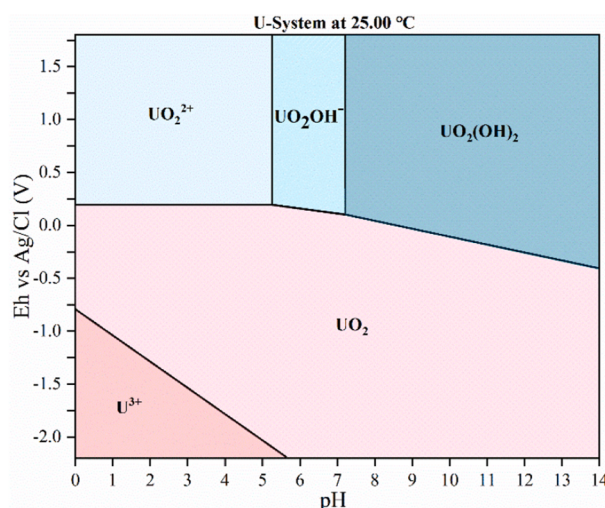


Fig. 5. Eh-pH phase diagram of uranium in solution (25°C , 1 bar total pressure, U concentration of 10 mg/L). (Thermodynamic database is accessed from HSC 9 software).

environments. Fig. 6b shows that uranium recovery rate improves with increasing initial pH. The recovery rate of uranium at pH = 1.65 or 2.00 is much higher than that at pH = 1.30. This enhancement can be attributed to the reduced competition from protons (H^+) at higher pH levels, which facilitates the migration and reduction of UO_2^{2+} toward the cathode. Additionally, the initial sulfate concentration of feedwater with higher pH value is lower, resulting in less $\text{UO}_2(\text{SO}_4)_2^{2-}$ but more $\text{UO}_2(\text{SO}_4)$ in the feedwater (Fig. S5), the $\text{UO}_2(\text{SO}_4)$ absorbed on AEM would be desorbed by H^+ in the strong acidic anode flow electrode (Fig. 6c), promoting uranium recovery in the anode.

In addition to uranium, the recovery rate of coexisting ions are also affected by initial feedwater pH (Fig. 6b). At higher pH values (1.65 and 2.00), the recovery rates of Fe^{3+} and Ca^{2+} dramatically increase. This is because the H^+ content in feedwater is much lower at initial pH of 1.65 or 2.00, but the amount of OH^- produced in cathode is close to that at initial pH of 1.30 due to the same charging voltage, resulting in higher cathode pH at higher initial feedwater pH, especially in the case of initial pH of 2.00, as shown in Fig. 6d. Fe^{3+} and Ca^{2+} tends to hydrolyze or form insoluble complexes, leading to a reduced mobility from the cathode to the spacer during discharging. Conversely, Na^+ presents a decreasing recovery rate with the increase of initial pH, due to the reduced competition from other ions. These results suggest that reasonably decreasing the cathode pH can enhance uranium selectivity recovery.

3.3. Migration and transformation mechanism of uranium

Based on the U concentration measured in the experiments in section 3.2.3 (initial U concentration of the feedwater is 100 mg/L), the percentage of U distributed in each part of the FCDI device was calculated. Fig. 7a shows the mass distribution of U in the FCDI operation. It is clear that U occurs at both cathode and anode. The reason is that U(VI) mainly occurs in the form of charge neutral $\text{UO}_2(\text{SO}_4)$ (55–65 %), followed by $\text{UO}_2(\text{SO}_4)_2^{2-}$ (5–25 %) and UO_2^{2+} (10 %–30 %) in sulfuric acid solution with $\text{pH} < 5$ (Fig. S6). In addition, it is seen from Fig. 7a that the proportion of U on AEM is higher than that on CEM. This is because the quaternary ammonium group on strong alkaline AEM could complex with SO_4^{2-} in the feedwater, and further complexes with the uncharged $\text{UO}_2(\text{SO}_4)$ in the feedwater during charging process (Arden and Wood, 1956), which was detailed in our previous work (Tang et al., 2025). The uncharged $\text{UO}_2(\text{SO}_4)$ absorbed on AEM is not susceptible to the electric field, as a result, it is difficult to migrate into the spacer during discharging process.

The U concentration in the electrolyte of anode and cathode is also shown in Fig. 7a. It is obvious that U concentration in anode electrolyte is much higher than that in cathode electrolyte after one cycle, though the content of $\text{UO}_2(\text{SO}_4)_2^{2-}$ is lower than that of UO_2^{2+} in the feedwater (Fig. S6). We measured the concentration of SO_4^{2-} in the anode flow electrode, and found that it increases with the number of charging-discharging cycles (Fig. S7). Then, the oxidation of graphite or water hydrolysis would occur to produce H^+ to maintain electroneutrality of the electrolyte in anode. The concentration of SO_4^{2-} in the electrolyte of anode could be considered as the concentration of H_2SO_4 . Previous studies (Gu et al., 2005; Masoud, 2022; Zagorodnyaya et al., 2013) have shown that sulfuric acid can desorb $\text{UO}_2(\text{SO}_4)$ from AEMs, enabling uranium recovery. Thus, part of $\text{UO}_2(\text{SO}_4)$ on AEM was desorbed by H_2SO_4 generated in anode into the electrolyte with increasing cycles.

The proportion of $\text{UO}_2(\text{SO}_4)_2^{2-}$ is low under acidic condition even though the sulfate content is high (Fig. S5), most of the $\text{UO}_2(\text{SO}_4)_2^{2-}$ entering anode chamber during charging process would be decomposed into uncharged $\text{UO}_2(\text{SO}_4)$ and/or UO_2^{2+} , as shown in reactions (9) and (10) (Arden and Wood, 1956). At the discharging phase, the polarity is reversed, UO_2^{2+} can be adsorbed on the electric double layer (EDL) of the anode carbon particles, only the unreacted $\text{UO}_2(\text{SO}_4)_2^{2-}$ migrates into the spacer due to the acceleration of electric field.

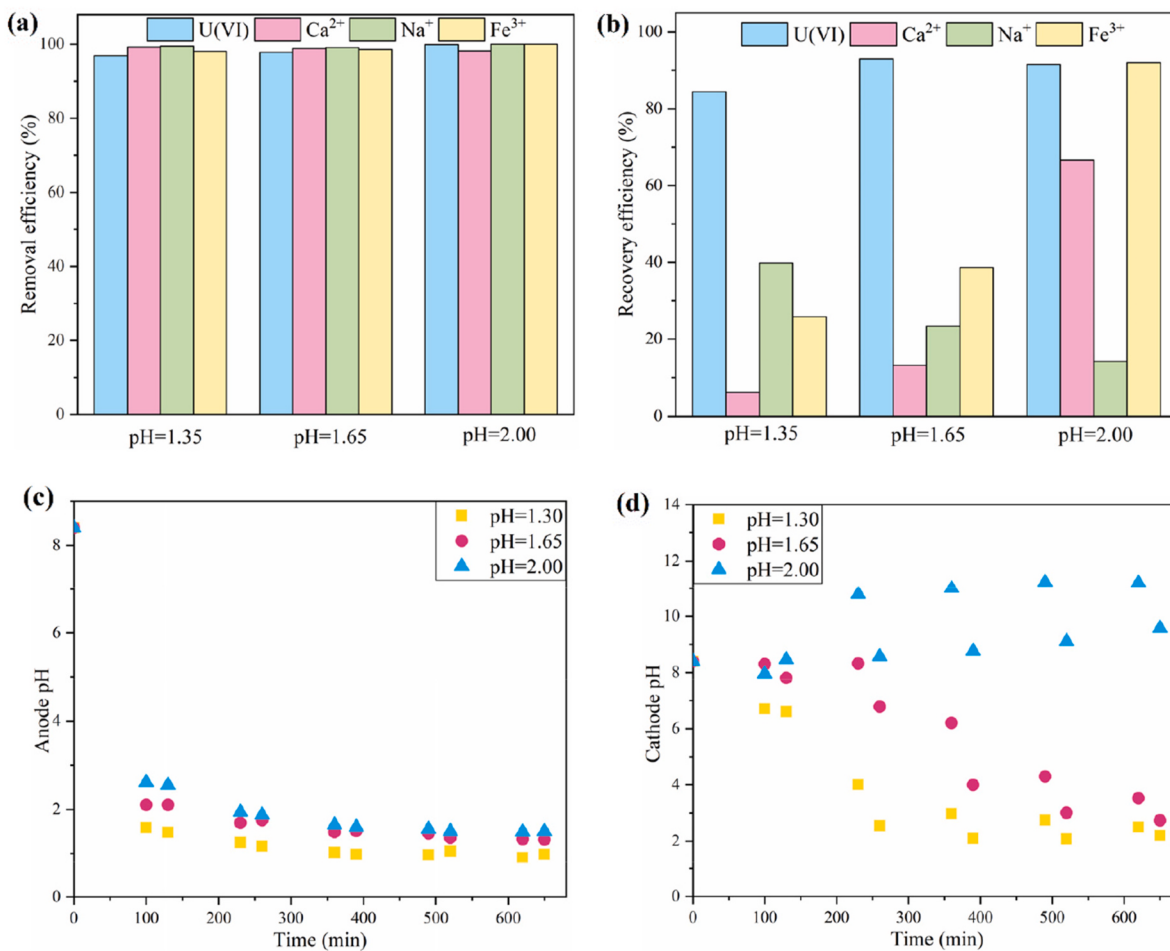


Fig. 6. (a) Removal efficiency of ions; (b) recovery rate of ions; (c) anode pH; (d) cathode pH under condition of different initial pH of feedwater. ($U_c = 3.6$ V, $t_c = 100$ min, $U_d = 0.2$ V, $t_d = 30$ min, HRT = 5min).

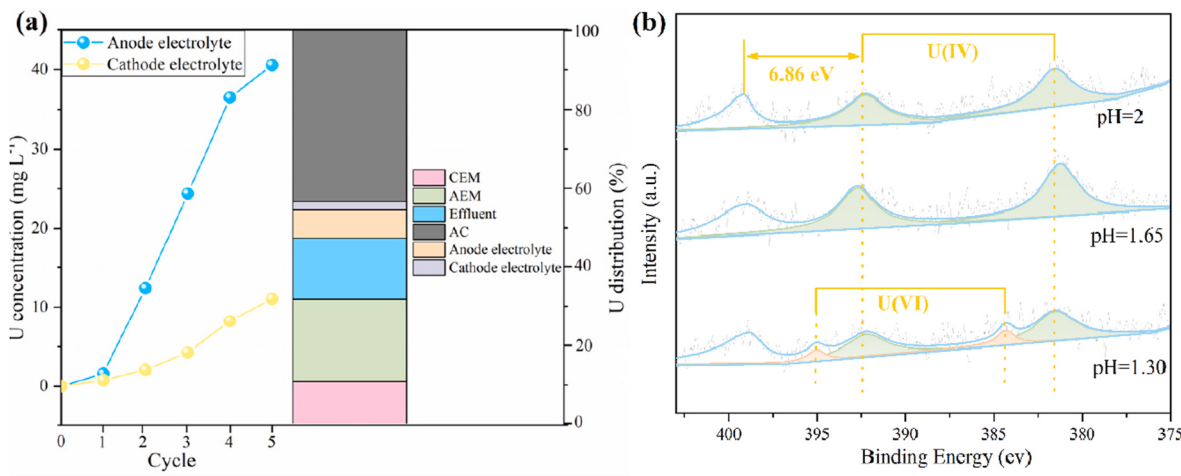


Fig. 7. (a) Mass distribution of U in FCDI components and (b) XPS spectrum of cathode carbon particles after five continuous charring-discharging cycles. ($U_c = 3.6$ V, $t_c = 100$ min, $U_d = 0.2$ V, $t_d = 30$ min, HRT = 5 min).



In order to reveal the valence change of uranium in the FCDI cell, we investigated the XPS spectra of carbon particles separated from the

cathode after five continuous cycles at different initial feedwater pH. Fig. 7b displays that the U4f peaks present in the XPS spectrum of carbon particles, indicating the successful combination of uranium on carbon particles. The peak at ~381.0 eV and ~392.0 eV is the U4f7/2 and U4f5/2 main peaks, respectively, while the peak at 398.8 eV is the satellite peak of U4f5/2. The separation between the two main peaks is

about 10.8 eV at initial pH of 1.30, 1.65 and 2.00, and there is a peak on the side of the higher binding energy. The space between the satellite peak and main peak of the U4f5/2 is 6.86 eV, suggesting the presence of U(IV) on the cathode carbon particles (Liu et al., 2019; Yuan et al., 2015). This is consistent with the previous studies, which have shown that U(VI) can be electrochemically reduced to UO_2 [U(IV)] when the voltage exceeds 0.9 V (Zhou et al., 2022). In addition, two small U(VI) peaks were detected on carbon particles on condition of an initial pH of 1.30. This likely represents a combination of (a) secondary oxidation of U(IV) to U(VI) in acidic media and (b) a minor fraction of incompletely reduced or adsorbed U(VI).

The above results show that uranium underwent a complex migration and transformation process in FCDI system during charging and discharging process, which can be schematically depicted by Fig. 8. At charging phase, UO_2^{2+} , H^+ and other competing cations (Ca^{2+} , Fe^{3+} , Na^+) migrate into the cathode, and then UO_2^{2+} , H^+ as well as Fe^{3+} are reduced to UO_2 , H_2 , and Fe^{2+} , respectively, due to the low electrode potential in cathode. By contrast, $\text{UO}_2(\text{SO}_4)_2^{2-}$, SO_4^{2-} and other anions transport to the anode, and some $\text{UO}_2(\text{SO}_4)_2^{2-}$ dissociates into $\text{UO}_2(\text{SO}_4)/\text{UO}_2^{2+}$ and SO_4^{2-} . A part of $\text{UO}_2(\text{SO}_4)$ on the AEM would be desorbed by H_2SO_4 into the anolyte. During discharging process, most of the SO_4^{2-} and competing cations migrate to the spacer due to the acceleration of electric field, while the UO_2^{2+} produced in the anode absorbs onto the EDL of electrode material.

3.4. Long-term stability

To evaluate the practical applicability and durability of the FCDI system, twelve consecutive charging-discharging cycles were conducted using real uranium-contaminated acidic groundwater collected from an uranium mining site in Xinjiang, China. The performance metrics, including removal and recovery efficiencies of uranium and coexisting ions, are shown in Fig. 9. It is seen that the FCDI system maintained high

removal efficiencies (>90 %) for U(VI), Fe^{3+} , Al^{3+} , Mg^{2+} , Na^+ , and K^+ throughout the cycling tests. The removal efficiency of Ca^{2+} is slightly lower, averaging around 85.45 %. Notably, all ions demonstrate improved removal performance after the first cycle. This phenomenon is attributed to the increase in flow electrode conductivity caused by the ion migration during the first charging phase, which reduces the internal resistance and enhances subsequent performance.

Fig. 9a shows that U recovery rate remains stable above 84.85 % even after twelve cycles, demonstrating the robust U recovery and electrochemical stability of the FCDI system. In contrast, the recovery rates of co-ions, particularly Al^{3+} and Fe^{3+} , shows an obvious downward trend with increasing cycles. For instance, Al^{3+} recovery rate decreases from 53.90 % in the first cycle to 27.67 % by the twelfth. The reason is that the hydrolysis of Al^{3+} and Fe^{3+} is reduced with the decreasing pH of the cathode flow electrode (Fig. S8), suppressing the recovery of Al^{3+} and Fe^{3+} during discharging. This result indicates that the selective recovery of uranium can be enhanced by adjusting the pH of the cathode flow electrode.

Although FCDI removes both cations and anions non-selectively from the spacer during charging, the net fate of uranium differs substantially from that of competing ions after discharging. Over 80 % of U is retained in the electrode suspensions and membrane, whereas Ca^{2+} , Na^+ , and Fe^{3+} are largely released back to the spacer effluent during discharge process. This effective selectivity arises from three mechanisms: (i) electrochemical reduction of U(VI) to insoluble UO_2 ($K_{sp} \approx 10^{-23}-10^{-24}$) on cathodic carbon particles, confirmed by XPS (Fig. 7b), and the reduction of Fe^{3+} ($K_{sp} \approx 4.0 \times 10^{-38}$) to soluble Fe^{2+} ($K_{sp} \approx 4.87 \times 10^{-17}$); (ii) decomposition of $\text{UO}_2(\text{SO}_4)_2^{2-}$ into uncharged $\text{UO}_2(\text{SO}_4)$ and/or UO_2^{2+} , which could be absorbed by carbon particles during discharging; and (iii) adsorption of $\text{UO}_2(\text{SO}_4)$ on AEM functional groups, followed by gradual desorption into the anolyte. Moreover, operation at a low discharging voltage ($U_d = 0.2$ V), which prevents re-oxidation and remobilization of UO_2 . These processes explain the negligible ASRR_d of

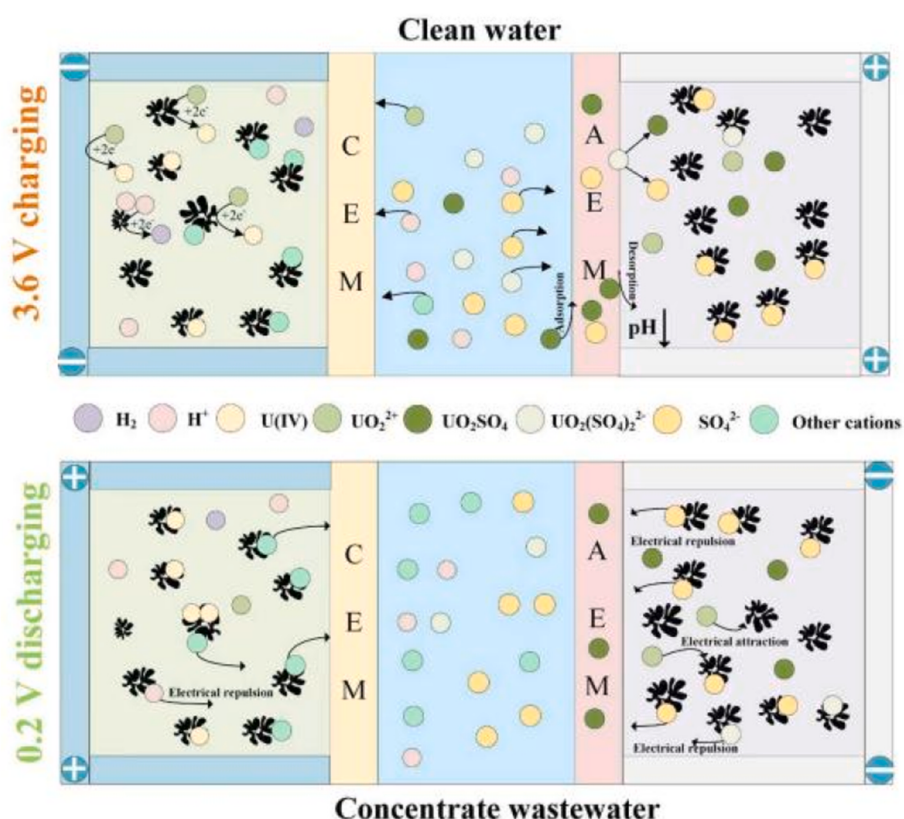


Fig. 8. Mechanism of uranium migration and transformation during charging and discharging.

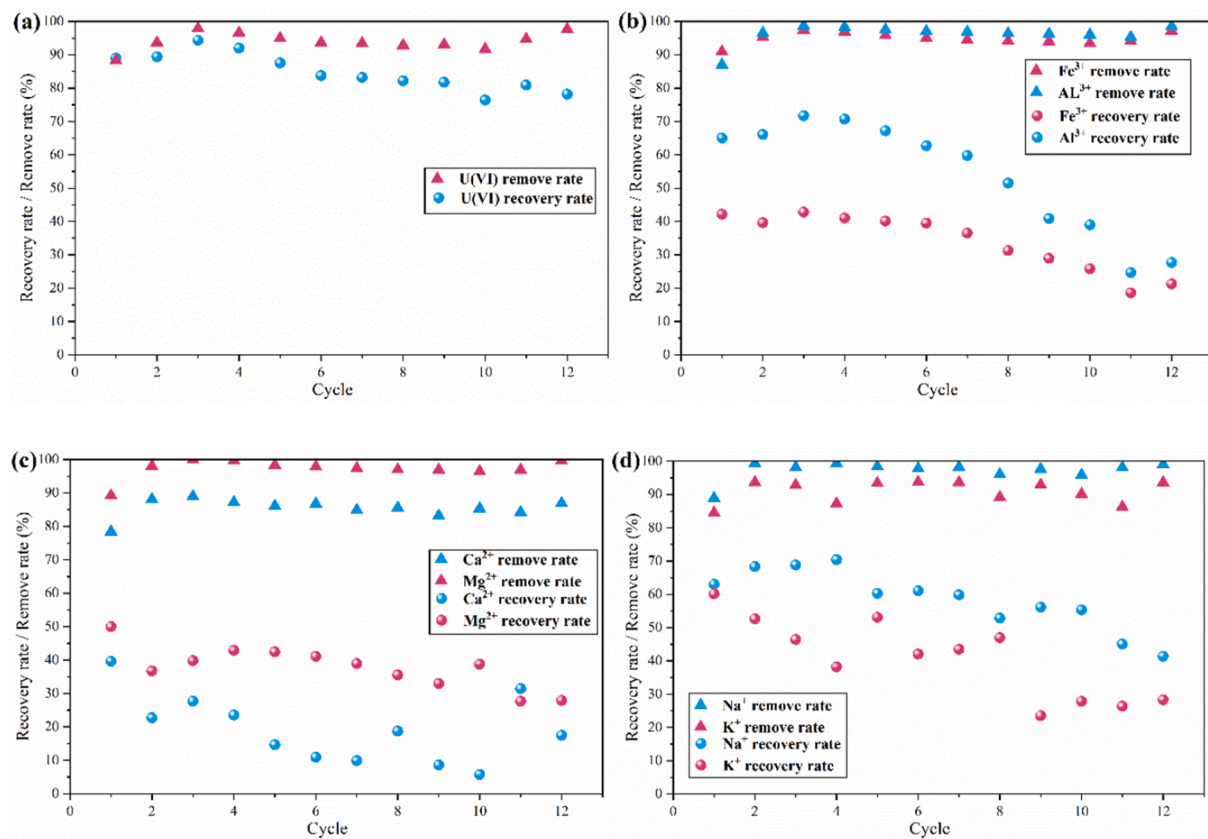


Fig. 9. (a) Recovery rate of U, (b) Recovery rate of Fe^{3+} and Al^{3+} , (c) Recovery rate of Ca^{2+} and Mg^{2+} , and (d) Recovery rate of Na^+ and K^+ .

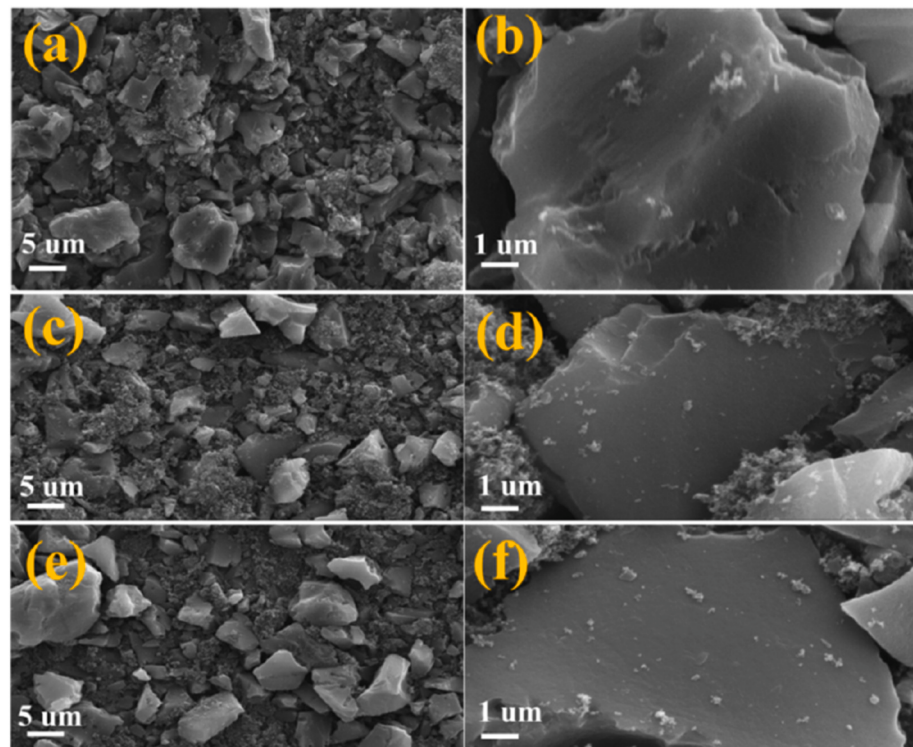


Fig. 10. (a-b) Initial electrode material; (c-d) anodic electrode material after 12 cycles; (e-f) cathodic electrode material after 12 cycles. ($U_c = 3.6 \text{ V}$, $t_c = 100 \text{ min}$, $U_d = 0.2 \text{ V}$, $t_d = 30 \text{ min}$, HRT = 5 min).

uranium (Fig. 2d) compared with the co-existing ions and demonstrate that FCDI, though non-selective in ion removal, achieves selective uranium recovery in consolidated electrode/anolyte and membrane adsorption phases.

Additionally, an increasing concentration of SO_4^{2-} in the anode electrolyte was observed over cycles, reaching 20.99 g/L after twelve cycles. This accumulation likely enhances the formation of $\text{UO}_2(\text{SO}_4)_2^{2-}$ (Fig. S5), which is prone to migrate to the spacer during discharging, potentially accounting for the slight reduction in uranium recovery rate. Nevertheless, the accumulation of sulfuric acid in the anode chamber also facilitates the desorption of $\text{UO}_2(\text{SO}_4)$ complexes from AEM, thereby aiding long-term uranium recovery.

The stability of the electrode materials was further confirmed by scanning electron microscopy (SEM), energy spectrum analysis (EDS), and FTIR analyses. SEM images (Fig. 10) reveals no significant morphological degradation of the activated carbon particles after twelve cycles. EDS spectra (Fig. S9) shows the presence of U and S on anode carbon particles, and the occurrence of U, Fe, Al, Ca, Mg, Na and K on cathode carbon particles, confirming ion-specific deposition patterns consistent with electrochemical behavior. Moreover, FTIR spectra (Fig. 11) demonstrated negligible changes in surface functional groups. These results indicate excellent physical and chemical stability of the carbon material during extended operation at $U_c = 3.6$ V.

To evaluate reversibility of membranes, we conducted preliminary rinsing tests, in which used AEM and CEM were soaked in 1~2% HNO_3 , significant uranium was eluted (Supplementary Table S3), while the membrane retained ion-exchange functionality. These results suggest that membrane fouling is not permanent, and that periodic acid rinsing could serve as a regeneration strategy. Nevertheless, irreversible binding or gradual degradation cannot be excluded over longer operation.

In addition to contaminant removal, our process enables the selective recovery of U with recovery rates exceeding 80% (Fig. 9a). This not only prevents long-term environmental risks associated with U mobility but also allows the reclamation of uranium resource in wastewater, aligning with the principles of sustainable resource use. Unlike traditional methods, the FCDI process does not require the addition of chemical reagents, avoiding secondary sludge generation. Moreover, the carbon-based flow electrodes exhibit excellent long-term stability over 12 continuous cycles (Figs. 10 and 11), reducing material consumption and waste generation. These results demonstrate FCDI as a promising and sustainable technology for simultaneous uranium remediation and resource recovery from strongly acidic groundwater.

However, there are still some issues should be addressed to promote industrial application. A portion of uranium adsorbed on the ion exchange membranes, especially AEM (Fig. 7a). Though it doesn't significantly affect the performance of membranes, it poses a practical challenge for full system recovery. As for the fraction of uranium retained on AEM after FCDI treatment, it can be desorbed using $\text{Na}_2\text{CO}_3/\text{NaHCO}_3$, while the uranium adsorbed on CEM could be desorbed using 2% HNO_3 . The soluble U-sulfate complexes released to the anolyte can be directed to conventional recovery steps such as precipitation or solvent extraction. Besides, there exist some parasitic electrochemical reactions due to the high charging voltage. We recommend (and in some cases applied) the following measures: (1) operate within an optimized voltage window (charging voltage minimized consistent with required removal rates and U_d kept as low as possible to prevent U re-oxidation); (2) improve flow-electrode conductivity (higher content of carbon or conductive additives) to reduce ohmic losses and lower required cell voltages; (3) apply pulse charging to decrease side reaction while maintaining net ion transport; (4) select carbon materials with greater oxidation resistance or protective surface treatments; and (5) use pre-treatment (e.g., pH adjustment) or periodic membrane cleaning (acid elution) to prevent fouling caused by Fe/Al hydrolysis. Additionally, upscaling the FCDI unit and coupling it with renewable energy sources (e.g., photovoltaic systems) holds promise for sustainable deployment in remote or off-grid mining regions.

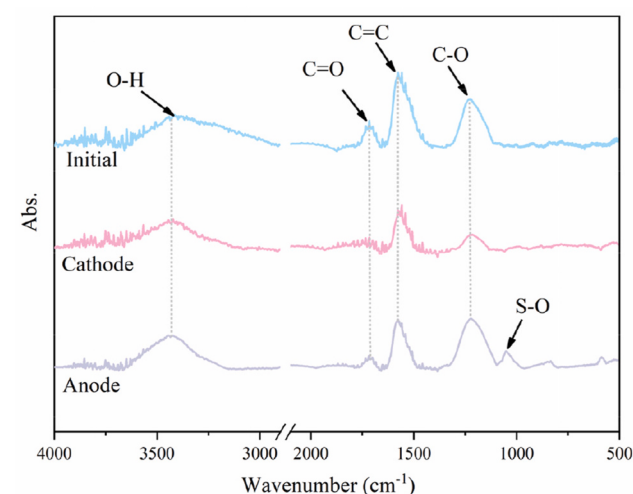


Fig. 11. FTIR spectrum of electrode material before and after the cycling experiments.

4. Conclusion

This study demonstrates the feasibility and effectiveness of using FCDI for the simultaneous removal and recovery of uranium from strongly acidic, sulfate-rich groundwater produced by AISL process. The FCDI system showed high removal efficiencies of uranium and coexisting ions (>90%) and a stable uranium recovery rate (>80%) across multiple charging-discharging cycles under optimal condition ($U_c = 3.6$ V, $t_c = 100$ min, $U_d = 0.2$ V, $t_d = 30$ min and HRT = 5 min). It is found that UO_2^{2+} is reduced to UO_2 on carbon particles in cathode, $\text{UO}_2(\text{SO}_4)_2^{2-}$ is decomposed into $\text{UO}_2(\text{SO}_4)$ or UO_2^{2+} and SO_4^{2-} in anode, besides, charge neutral $\text{UO}_2(\text{SO}_4)$ adsorbs on AEM during charging. During the discharging process, UO_2 in cathode is hardly affected by the electric field, while the coexisting cations quickly move out of cathode chamber because of electrorepulsion. The UO_2^{2+} in anode is adsorbed in the EDL of carbon particles, and the remained $\text{UO}_2(\text{SO}_4)_2^{2-}$ in anode migrates to the spacer due to electrorepulsion. $\text{UO}_2(\text{SO}_4)$ adsorbed on AEM can be desorbed as the concentration of H^+ in the anodic electrolyte increases. Beyond technical performance, the sustainability of FCDI process is supported by its minimal secondary waste production due to chemical-free operation, and the ability to recover U as a valuable resource, aligning with principles of circular economy and reducing environmental burden. These results demonstrate that FCDI is a promising and sustainable method for the removal and recovery of uranium from strong acidic contaminated water. The selective recovery of uranium could be further improved by optimizing the operating parameters in the future.

CRediT authorship contribution statement

Zhipeng Tang: Writing – original draft, Software, Investigation, Formal analysis, Data curation. **Yongmei Li:** Writing – review & editing, Writing – original draft, Methodology, Investigation, Funding acquisition, Conceptualization. **Kaixuan Tan:** Writing – review & editing, Validation, Formal analysis. **Chunguang Li:** Software. **Zhenzhong Liu:** Data curation. **Chong Zhang:** Data curation. **Haiwei Shi:** Investigation. **Le Ouyang:** Investigation. **Longcheng Liu:** Writing – review & editing.

Declaration of competing interest

The authors declare that they have no known competing financial interests or personal relationships that could have appeared to influence the work reported in this paper.

Acknowledgments

We would like to thank the National Natural Science Foundation of China (52404130, U1703123) and the Natural Science Foundation of Hunan Province, China (2023JJ40522) for their support.

Appendix A. Supplementary data

Supplementary data to this article can be found online at <https://doi.org/10.1016/j.jclepro.2025.146724>.

Data availability

Data will be made available on request.

References

- Arden, T.V., Wood, G.A., 1956. Adsorption of complex anions from uranyl sulphate solution by anion-exchange resins. *J. Chem. Soc.* 0, 1596–1603.
- Bhargava, S.K., Ram, R., Powneby, M., 2015. A review of acid leaching of uraninite. *Hydrometallurgy* 151, 10–24.
- Berenice, M.A., Federico, C.Z., Luis, O.F., René, A., Fernando, F.R., 2021. Electrochemical study of iron deposit in acid media for its recovery from spent pickling baths regeneration. *J. Electroanal. Chem.* 901, 115805. <https://doi.org/10.1016/j.jelechem.2021.115805>.
- Chen, T.Q., Xu, L.Q., Wei, S., Fan, Z.Q., Qian, R.B., Ren, X.L., Zhou, G., Yang, H.Q., Wu, J.Y., Chen, H.B., 2022. Ammonia-rich solution production from coal gasification gray water using Chemical-free flow-electrode capacitive deionization coupled with a monovalent cation exchange membrane. *Chem. Eng. J.* 433, 133780. <https://doi.org/10.1016/j.cej.2021.133780>.
- Gu, B., Ku, Y.K., Brown, G.M., 2005. Sorption and desorption of perchlorate and U(VI) by strong-base anion-exchange resins. *Environ. Sci. Technol.* 39 (3), 901–907. <https://doi.org/10.1021/es049121f>.
- Guo, D.G., Yan, C.P., Huang, B., Jin, T.X., Liu, Z.R., Qian, Y., 2025. Combining electrosorption and electrochemical reduction mechanisms for uranium removal using 1,2,3,4-butane tetracarboxylic acid-modified MIL-101: an in-depth exploration of uranyl–adsorbent interactions. *Inorg. Chem.* 64, 1777–1787.
- Heshmati, H., Torab-Mostaedi, M., Ghanadzadeh Gilani, H., Heydari, A., 2015. Kinetic, isotherm, and thermodynamic investigations of uranium (VI) adsorption on synthesized ion-exchange chelating resin and prediction with an artificial neural network. *Desalination Water Treat.* 55 (4), 1076–1087.
- He, C.Y., Tan, K.X., Li, Y.M., Liu, Z.Z., Zhang, Q.L., Li, D., Liu, Z., 2021. Pollution characteristics and mechanism of groundwater of acid and CO₂ in-situ leaching mining area of uranium deposit in Xinjiang, China. *Nonferrous Met.* 6, 53–59.
- Huang, J., Liu, Z.R., Huang, D.J., Jin, T.X., Qian, Y., 2022. Efficient removal of uranium (VI) with a phytic acid-doped polypyrrole/carbon felt electrode using double potential step technique. *J. Hazard Mater.* 433, 128775.
- Jeon, S.I., Park, H.R., Yeo, J.G., Yang, S.C., Cho, C.H., Han, M.H., Kim, K.D., 2013. Desalination via a new membrane capacitive deionization process utilizing flow-electrodes. *Energy Environ. Sci.* 6 (5), 1471–1475.
- James, G.S., 2004. Lange's Handbook of Chemistry the sixteenth edition, the United States of America.
- Ke, P.C., Wu, T.N., Liu, Y.J., Zhao, B., Zhong, T.T., Sun, Z.X., Wang, M.B., 2023. Progress in treatment technology of uranium-containing wastewater. *Ind. water Treat.* 43 (9), 20–31.
- Liao, X., Ma, H., Wang, R.u., Shi, B.i., 2004. Adsorption of UO₂⁺ on tannins immobilized collagen fiber membranes. *J. Membr. Sci.* 243 (1–2), 235–241.
- Lim, J., Lee, S., Lee, H., Hong, S., 2024. Energetic comparison of flow-electrode capacitive deionization and membrane technology: assessment on applicability in desalination fields. *Environ. Sci. Technol.* <https://doi.org/10.1021/acs.est.4c00672>.
- Liu, T., Yuan, J.L., Zhang, B., Liu, L.M., Meng, Y., Yin, S.F., Liu, C.B., Luan, F.B., 2019. Removal and recovery of uranium from groundwater using direct electrochemical reduction method: performance and implications. *Environ. Sci. Technol.* 53 (24), 14612–14619. <https://doi.org/10.1021/acs.est.9b06790>.
- Luo, K.Y., Niu, Q.Y., Zhu, Y., Song, B., Zeng, G.M., Tang, W.W., Ye, S.J., Zhang, J., Duan, M.B., Xing, W.L., 2020. Desalination behavior and performance of flow-electrode capacitive deionization under various operational modes. *Chem. Eng. J.* 389, 124051. <https://doi.org/10.1016/j.cej.2020.124051>.
- Ma, J., Zhai, C.X., Yu, F., 2023. Review of flow electrode capacitive deionization technology: research progress and future challenges. *Desalination* 564, 116701.
- Ma, J.X., Zhang, Y.M., Collins, R.N., Tsarev, S., Aoyagi, N., Kinsela, A.S., Jones, A.M., Waite, T.D., 2019. Flow-electrode CDI removes the uncharged Ca-UO₂-CO₃ ternary complex from brackish potable groundwater: complex dissociation, transport, and sorption. *Environ. Sci. Technol.* 53 (5), 2739–2747. <https://doi.org/10.1021/acs.est.8b07157>.
- Ma, J.X., Ma, J.J., Zhang, C.Y., Song, J.K., Dong, W.J., Waite, T.D., 2020. Flow-electrode capacitive deionization (FCDI) scale-up using a membrane stack configuration. *Water Res.* 168, 115186. <https://doi.org/10.1016/j.watres.2019.115186>.
- Masoud, A.M., 2022. Sorption behavior of uranium from sulfate media using purolite A400 as a strong base anion exchange resin. *Int. J. Environ. Anal. Chem.* 102 (13), 3124–3146. <https://doi.org/10.1080/03067319.2020.1763974>.
- Maxim, S., Alexander, Z., Graham, J., 2016. In situ recovery, an alternative to conventional methods of mining: exploration, resource estimation, environmental issues, project evaluation and economics. *Ore Geol. Rev.* 79, 500–514.
- Nassrullah, H., Fatima Anis, S., Hashaikeh, R., Hilal, N., 2020. Energy for desalination: a state-of-the-art review. *Desalination* 491, 114569.
- OECD-NEA & IAEA, 2020. Uranium 2020: resources, production and demand. Red book 2020. In: Redbook NEA No. 7551 Nuclear Energy Agency and the International Atomic Energy Agency.
- Santos, E.A., Ladeira, A.C.Q., 2011. Recovery of uranium from mine waste by leaching with carbonate-based reagents. *Environ. Sci. Technol.* 45 (8), 3591–3597.
- Song, W., Liu, M., Hu, R., Tan, X., Li, J., 2014. Water-soluble polyacrylamide coated-Fe₃O₄ magnetic composites for high-efficient enrichment of U(VI) from radioactive wastewater. *Chem. Eng. J.* 246, 268–276.
- Tang, Z.P., Li, Y.M., Tan, K.X., Wang, G.H., Li, C.G., Liu, L.C., Liu, Z.Z., 2025. Efficient removal of uranium and sulfate in acid contaminated groundwater by flow electrode capacitive deionization. *Desalination* 594, 118304.
- Tauk, M., Bechelany, M., Sistat, P., Habchi, R., Cretin, M., Zaviska, F., 2024a. Ion-selectivity advancements in capacitive deionization: a comprehensive review. *Desalination* 572, 117146. <https://doi.org/10.1016/j.desal.2023.117146>.
- Tauk, M., Cretin, M., Bechelany, M., Sistat, P., Zaviska, F., 2024b. Capacitive deionization: a promising water treatment and desalination technology. In: Jlassi, K., Oturan, M.A., Ismail, A.F., Chehimi, M.M. (Eds.), *Clean Water: next Generation Technologies. Advances in Science, Technology & Innovation*. Springer International Publishing, pp. 25–40. https://doi.org/10.1007/978-3-031-48228-1_2.
- Walha, K., Amar, R.B., Firdaous, L., Quéméneur, F., Jaouen, P., 2007. Brackish groundwater treatment by nanofiltration, reverse osmosis and electrodiagnosis in Tunisia: performance and cost comparison. *Desalination* 207 (1/2/3), 95–106.
- Wang, S.F., Jiang, J.L., He, X., Yang, S.L., Wu, H.X., Qin, Z., Chu, M.F., Zhang, Z.J., Liao, J.S., Wang, X.L., 2022. Research progress of SERS on uranyl ions and uranyl compounds: a review. *J. Mater. Chem. C* 10 (11), 4006–4018. <https://doi.org/10.1039/D1TC05154G>.
- Xia, Q.Y., Wang, X., Zeng, Q., Guo, D.Y., Zhu, Z.H., Chen, H.Y., Dong, H.L., 2020. Mechanisms of enhanced antibacterial activity by reduced chitosan-intercalated nontronite. *Environ. Sci. Technol.* 54 (8), 5207–5217.
- Xu, L.Q., Ding, R., Mao, Y.F., Peng, S., Li, Z., Zong, Y., Wu, D.L., 2021. Selective recovery of phosphorus and urea from fresh human urine using a liquid membrane chamber integrated flow-electrode electrochemical system. *Water Res.* 202, 117423. <https://doi.org/10.1016/j.watres.2021.117423>.
- Yang, S.X., Yan, C.P., Huang, B., Jin, T.X., Guo, D.G., Xiao, M.N., Qian, Y., 2025. PBTCA-modified self-crosslinked chitosan gels for efficient electrosorption of uranium from wastewater. *Desalination* 612, 118984.
- Ye, Y., Jin, J., Han, W., Miao, S.Y., Feng, Y.Y., Qin, Z.M., Tang, X., Li, C., Chen, Y.L., Chen, F., Wang, Y.H., 2023. Spontaneous electrochemical uranium extraction from wastewater with net electrical energy production. *Nature water* 1, 887–898. <https://doi.org/10.121203/rs.rs-1715307/v1>.
- Yin, H.Y., Liu, L.H., Ma, J.X., Zhang, C.Y., Qiu, G.H., 2023. Efficient removal of As(III) from groundwaters through self-alkalization in an asymmetric flow-electrode electrochemical separation system. *Water Res.* 246, 120734. <https://doi.org/10.1016/j.watres.2023.120734>.
- Yuan, K., Ilton, E.S., Antonio, M.R., Li, Z.R., Cook, P.J., Becker, U., 2015. Electrochemical and spectroscopic evidence on the one-electron reduction of U(VI) to U(V) on magnetite. *Environ. Sci. Technol.* 49 (10), 6206–6213. <https://doi.org/10.1021/acs.est.5b00025>.
- Zagorodnyava, A.N., Abisheva, Z.S., Sharipova, A.S., Sadykanova, S.E., Bochevskaya, Y.G., Atanova, O.V., 2013. Sorption of rhenium and uranium by strong base anion exchange resin from solutions with different anion compositions. *Hydrometallurgy* 131–132, 127–132. <https://doi.org/10.1016/j.hydromet.2012.11.003>.
- Zhang, C.Y., Ma, J.X., Song, J.Y., He, C., Waite, T.D., 2018. Continuous Ammonia recovery from wastewaters using an integrated capacitive flow electrode membrane stripping system. *Environ. Sci. Technol.* 52 (24), 14275–14285. <https://doi.org/10.1021/acs.est.8b02743>.
- Zhang, C.Y., Ma, J.X., Waite, T.D., 2019. Ammonia-rich solution production from wastewater using chemical-free flow-electrode capacitive deionization. *ACS Sustain. Chem. Eng.* 7 (7), 6480–6485. <https://doi.org/10.1021/acscuschemeng.9b00314>.
- Zhang, C.Y., Ma, J.X., Wang, M., Sun, J.Y., Waite, T.D., 2020. Evaluation of long-term performance of a continuously operated flow-electrode CDI system for salt removal from brackish waters. *Water Res.* 173, 115580. <https://doi.org/10.1016/j.watres.2020.115580>.
- Zhang, C.Y., Ma, J.X., Wu, L., Sun, J.Y., Wang, L., Li, T.Y., Waite, T.D., 2021. Flow electrode capacitive deionization (FCDI): recent developments, environmental applications, and future perspectives. *Environ. Sci. Technol.* 55 (8), 4243–4267.
- Zhao, E.Y., Lv, H., Fan, J.H., Zhang, H.P., Wu, S.K., Yu, Y., Yang, Y.Q., Mei, S.X., 2025. Iron-carbon composite as flow electrode active material for highly efficient electrosorption of uranium from radioactive wastewater. *Separ. Purif. Technol.* 354, 128405. <https://doi.org/10.1016/j.seppur.2024.128405>.
- Zhong, L.J., Hu, S.J., Wu, D., Zhang, M.Y., Liu, H., Liu, Y., 2024. Simultaneously converting synthetic fresh urine into high-quality artificial phosphate ores and urea solution: a novel coupled system of electrochemical selective separation plus

- induced precipitation. *Separ. Purif. Technol.* 346, 127550. <https://doi.org/10.1016/j.seppur.2024.127550>.
- Zhou, J., Zhang, X., Zhang, Y., Wang, D., Zhou, H., Li, J., 2022. Effective inspissation of uranium (VI) from radioactive wastewater using flow electrode capacitive deionization. *Separ. Purif. Technol.* 283, 120172.
- Zhou, Y., Li, G., Xu, L., Liu, J., Sun, Z., Shi, W., 2020. Uranium recovery from sandstone-type uranium deposit by acid in-situ leaching—an example from the Kujieertai. *Hydrometallurgy* 191, 105209.